ESTIMATING LANDSLIDE-INDUCED RIVERBED ROUGHNESS VARIATION BY USING LIDAR DATA

Mon-Shieh Yang
Department of Earth Sciences, National Cheng Kung University, Tainan City, Taiwan, R.O.C

Ming-Chee Wu
Department of Earth Sciences, National Cheng Kung University, Tainan City, Taiwan, R.O.C.

Jin-King Liu
Secretary General, Taiwan Group on Earth Observations, Taiwan, R.O.C

ESTIMATING LANDSLIDE-INDUCED RIVERBED ROUGHNESS VARIATION BY USING LIDAR DATA

Mon-Shieh Yang[1], Ming-Chee Wu[1], and Jin-King Liu[2]

Key words: morphological analysis, surface roughness, digital elevation model, light detection and ranging.

ABSTRACT

With advancements in the efficiency and accuracy of investigation techniques and equipment, remote sensing technologies have been widely used to investigate river conditions. Quantifying the morphology along a river channel was difficult before airborne laser altimetry technology, light detection and ranging (LiDAR), was introduced, facilitating the collection of high-resolution, highly accurate topographical data. This study adopted airborne LiDAR data for analyzing and recognizing riverbed morphology. The roughness index was defined as the standard deviation of a residual topography. A variable moving-window was used to derive a smoothed digital elevation model (DEM). According to the roughness index, the residual topography was the difference between the original and smoothed DEMs. Roughness data derived from different reaches of a predisaster riverbed were compared with data derived from a postdisaster riverbed. The experimental results showed that the upper reaches exhibited higher roughness values than did the lower reaches. Thus, the relief of the postdisaster riverbed surface was near the derived smoothed relief. Such characteristics were reflected in the major differences evaluated through slope measurements in the riverbed morphological analysis; the position of the peak value changed after the disaster. An integrated plane-wise fluvial circumstance of a river watershed area was rapidly and accurately constructed, and this study concluded that these remote sensing techniques are vital in facilitating traditional surveys for regional investigations.

I. INTRODUCTION

Geomorphometry, which Chorley [3] defined as the science "which treats the geometry of the landscape," and quantitative procedure for quantifying the land surface, attempts to describe quantitatively the form of the land surface. In general, roughness refers to the irregularity of a topographic surface. Terrain roughness can be measured according to significant wavelengths. The significant wavelengths of topography are called grains or texture, whereas amplitudes associated with these wavelengths correspond to the concept of relief. The relationship between the horizontal and vertical dimensions of the topography is reflected in the land slope and dispersion of the slope magnitude and orientation, whereas the vertical distribution of mass under the topographic surface relates to hypsometry [12].

According to previous studies, evaluating the surface roughness by using light detection and ranging (LiDAR) data has been verified to facilitate detecting landslide areas [2, 4, 6, 14]. However, the surface roughness of a landform depends on the material properties, processes acting upon it, and the time elapsed since formation. River characteristics have played a crucial role in using hydrological models [13]. Sediments supplied from landslides may affect the river channel-morphology changes in various reaches or at different magnitudes; thus, riverbed morphology is related to disaster events. Benda and Dunne [1] analyzed the transportation of debris-flow sediment in first- and second- order channels, predicting the landslides in different channel reaches for the next 3000 years. The aim of the present study was to evaluate the data derived by using a multitemporal LiDAR digital elevation model (DEM) as a quantitative tool when a disaster occurred. Airborne LiDAR data were adopted to analyze and reveal riverbed morphology and rapidly and accurately construct an integrated plane-wise fluvial circumstance of a river watershed area.

II. STUDY AREA

1. Study Area

The study area, covering an area of 5.5×7 km^2, is located in the northeastern part of Kaohsiung City, Taiwan, and is
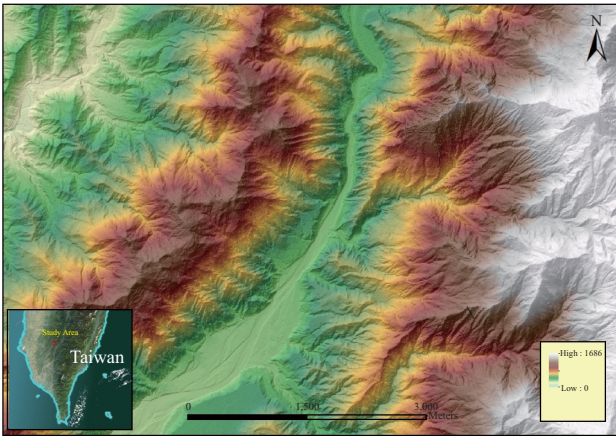
Fig. 1. Predisaster LiDAR DEM of the study area (Hsiaolin village).

situated in the sub-basin of the Kao-Ping Catchment (Fig. 1). Highly accurate, high-resolution airborne LiDAR images of the Kao-Ping Catchment were used to analyze and evaluate the predisaster and postdisaster riverbed roughnesses.

2. Landslide Event

Hsiaolin village, located in the northeastern part of Kaoh-siung City, sustained heavy damage during a catastrophic landslide event in August 2009. The Hsiaolin landslide, in-duced by Typhoon Morakot, was recognized as a wedge-type slope failure. The failure wedge was created by a N26°W/22°W bedding plane of Pliocene-Miocene Tangenshan sand-stone and a N80°E/84°N high-angle fracture; thus, a slide oriented in the west-southwesterly direction was generated [10].

3. Regional Geological Setting

The riverbed geological setting of the Hsiaolin village reach primarily comprises alternating sandstone and shale. Severe landslides occur after typhoons and rainfalls, particularly in areas near river banks and the main local highway.

III. PROCESSING METHODOLOGY

In some hydro-climatic regions, channel adjustment is strongly induced by colluvium sediment inputs (and thus, an imposed sediment size distribution) to channels through land-slides and debris flows. In these regions, the climatic influence on the network-wide distribution of step-pool channels may be closely linked to climatological events that deliver sediment to channels through mass movement. The amount and frequency of colluvium material delivery to channels may directly influ-ence the effectiveness of channel- forming events [5]. Mont-gomery and Buffington [15] distinguished between bedrock and alluvial channels in forested drainages by using slope-area plots. The roughness configurations or energy-dissipating fea-tures that distinguish these channel types reflect downstream changes in the sediment supply that are relative to capacity.

1. Topographic Data

The materials used in this study include an airborne LiDAR-DEM and the derived roughness data. The LiDAR-DEM was derived from point clouds and then resampled into 1-m grids. The LiDAR data were collected both before and after the Typhoon Morakot disaster, which occurred in August 2009.

2. Surface Roughness

The surface roughness is an expression of the topographic surface variability at a given scale. The roughness is deter-mined using surface-elevation values, and can be used to characterize landforms according to various scales [11]. In remote sensing, the roughness can also be quantified using the electromagnetic radiation reflections (i.e., ranging from specular to diffuse) from landform surfaces. A single defini-tion of surface roughness may be insufficient. In this study, surface roughness is treated as a geomorphometric variable, not a parameter. A variable is a measurable property of a phenomenon (e.g., slope angle), whereas a parameter is a summary measurement of the characteristics of a population (e.g., mean slope angle) [7]. Several methods have been de-veloped for defining, calculating, and applying surface rough-ness [2, 6].

3. Slope-Gradient Index

As previously mentioned, a landscape can be treated as a measurable phenomenon. The landforms of the surface roughness are mostly quantified through slope measurements; the slope is the rate of change in elevation. Slopes are re-garded as the most vital geomorphic parameters because they can be used to describe the relief and structure of the land surface [17]. A simple definition of a slope is

$$S = \arctan \sqrt{f_x^2 + f_y^2} \qquad (1)$$

where f_x and f_y defined in Eq. (2) are the gradients at W–E and N–S directions, respectively.

Z_7	Z_8	Z_9
Z_4	Z_5	Z_6
Z_1	Z_2	Z_3

$$f_x = \frac{(z_3 - z_1) + 2(z_6 - z_4) + (z_9 - z_7)}{8 \times cell\ size}$$

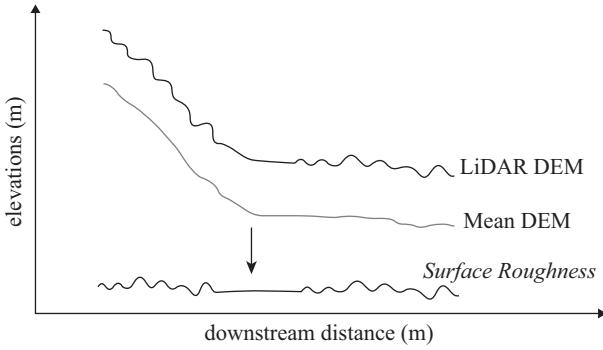$$f_y = \frac{(z_7 - z_1) + 2(z_8 - z_2) + (z_9 - z_3)}{8 \times cell\ size} \qquad (2)$$

Fig. 2. Surface roughness is calculated as the difference between LiDAR-DTM and mean DTM (modified from Cavalli *et al*. [2]).

Fig. 3. Two roughness index measurements: (a) Slope-Gradient; (b) Slope-Based.

where *z* is the topographic elevation. An algorithm developed by Sharpnack and Akin [16] and modified by Horn [8] uses eight grid points to calculate each gradient value by using a 3 × 3 moving window. This algorithm applies a third-order finite-difference technique that involves using the eight neighboring elevation values bordering the central elevation cell. This algorithm was validated using lower root mean square residuals in topographic analysis [17].

4. Slope-Based Roughness Index

In this study, the roughness index was defined as the standard deviation of the residual topography (Fig. 2). The variable moving window (5 × 5, five times the grid size of the original DEM) was used to derive the smoothed DEM, and the residual topography was the difference between an original and the smoothed DEM. Each cell corresponded to the mean DEM value of the 25 neighboring cells. The interval of the moving window for the roughness index was also determined using 5 × 5 cells; these values were considered to identify the upper limits of the analysis. The upper range of the limits corresponded to the river topography characteristics between 2.5 m to 5 m [2, 9].

Some studies have determined the relationship between the standard deviation of the residual topography and the riverbed roughness [2]. The formula is expressed as follows:

$$r = \sqrt{\frac{\sum_{i=1}^{25}(x_i - x_a)}{25}} \quad (3)$$

where *r* is the roughness index and also the standard deviation of the residual topography, x_i represents the value of the specific cell, x_a is the mean value corresponding to the specific cell (x_i), and 25 represents the number of the 5 × 5 neighboring cell value of the DEM.

The spatial variability of geomorphometric variables is crucial; knowing that an area is rougher or smoother than another is inadequate; instead, the degree and position of this difference must be determined because the degree and position
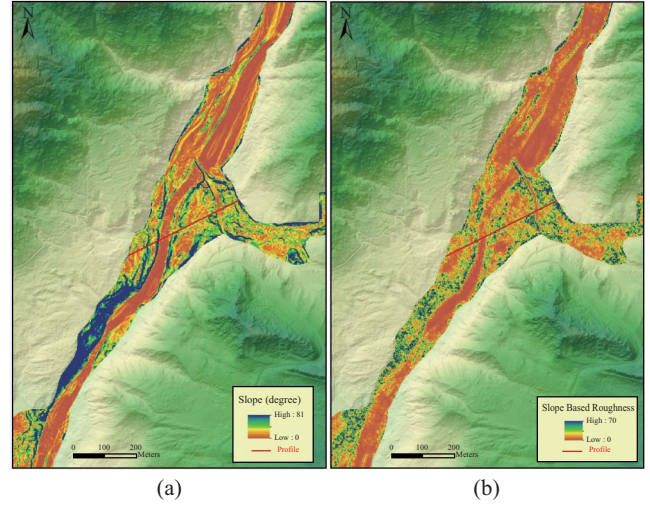
may be related to geological features such as lithological boundaries and tectonic structures [7].

The surface roughness index was derived from the LiDAR-DEM by using the standard deviation of the residual topography (*r*), and the roughness index was also used to generate the slope, which was then compared with the elevation-based slope. An algorithm of the third-order finite difference weighted by the reciprocal of the squared distance was used to assess the slope gradient.

$$S_r = \arctan\sqrt{f_x^2 + f_y^2}$$

$$f_x = \frac{(r_3 - r_1) + 2(r_6 - r_4) + (r_9 - r_7)}{8 \times cell\ size}$$

$$f_y = \frac{(r_7 - r_1) + 2(r_8 - r_2) + (r_9 - r_3)}{8 \times cell\ size} \quad (4)$$

where *r* is the standard deviation of the residual topography. The slope-based roughness was then computed in a 3 × 3 moving window.

5. River Change Characteristics Analysis

Analysis of changes in the riverbed area can provide essential information on the disaster. The analysis was performed by calculating the change in area between predisaster and postdisaster periods. The results revealed three statuses in the riverbed (i.e., gained, unchanged, and lost). Furthermore, a cross-sectional profile (Fig. 3) survey was conducted to assess the riverbed morphology change.

IV. RESULTS AND DISCUSSION

The slope-based roughness index was used for the predisaster and postdisaster analyses. Different river reaches were
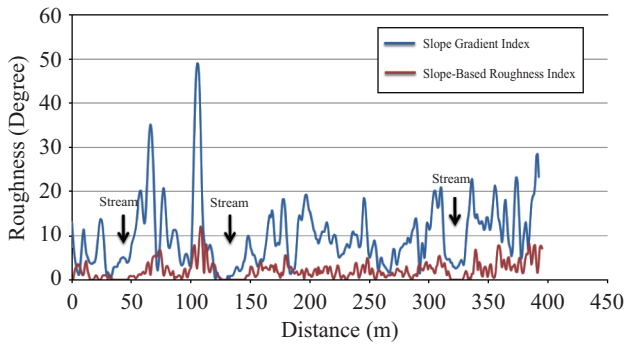
Fig. 4. Comparison of roughness indices in different river reaches.

compared using this method, and slope-gradient and surface-roughness indices were included in the comparison.

The results indicated that both methods reflected the variability of a topographic surface. Fig. 4 indicates that the stream topography in the slope-gradient and slope-based roughness indices reveal a substantial curve feature that corresponds in streams and flood land areas. However, the slope-gradient index at a stream boundary exhibits a higher value than that of the slope-based roughness index, indicating that the slope-based roughness index reveals smoother reflections than the slope-gradient index does. In addition, the slope-gradient index can reflect only the peak value clearly; however, the slope-based roughness index can depict more detailed curvilinear feature variations in topographic characteristics.

Both indices exhibit an increasing tendency in roughness when topographic breaks occur. The slope-gradient index in particular appears to be more sensitive than the slope-based roughness index does when the break point appears. Figs. 4 and 5 depict substantial differences in the spectrum profiles; as mentioned, the slope index shows a higher amplitude than does the roughness index in the vertical dimension. In uniform areas where the slope value is less than 10° (Fig. 4), the slope-based roughness index appears smoother than the slope-gradient index does; however, the slope-based roughness index reveals more detailed variability of topographic features and reflects a continuous relief.

Fig. 5 shows the box plots for the slope-based and slope-gradient roughness indices. Fig. 5(a) depicts the predisaster (2005) and postdisaster (2010) slope-gradient indices, indicating that they depict the same topographic features for the upper river and lower river reaches. Thus, that the slope in the two reaches decreased after the disaster, and the highest values for the slope-gradient and slope-based roughness indices decreased rapidly because of the increased elevations in these reaches. This increase may be attributed to the landslide materials transported from the upper reach and the increased flooding area.

The major difference between the slope-gradient index and the slope-based roughness index on riverbed measurement was determined through analysis (Fig. 5). For the predisaster

Table 1. Typhoon event induced flooding area and roughness change.

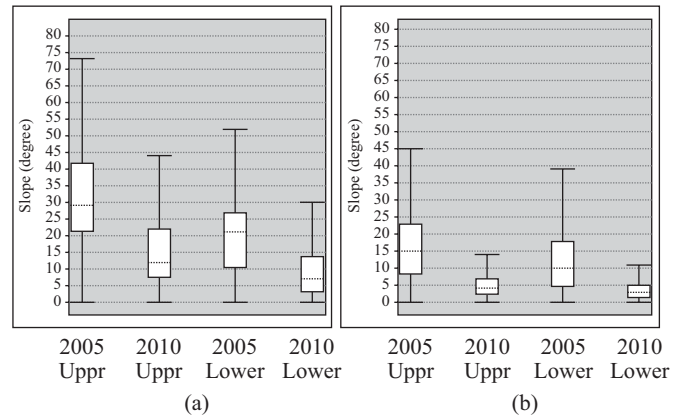|	Pre-disaster (2005)	Post-disaster (2010)	Change Rate
Area (m^2)	1614029	2631741	63%
Mean Slope (degree)	7.6	6.2	-22%

Fig. 5. Box plots for roughness measures of different river reaches: 2005, predisaster; 2010, postdisaster. (a) Slope Gradient Index; (b) Slope-Based Roughness Index.
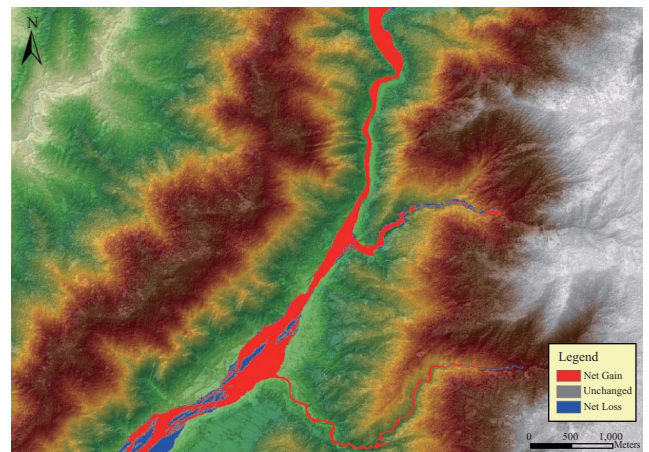

Fig. 6. Materials gained and lost in the riverbed.

and postdisaster periods, the slope-based roughness method obtained a smoother value than that of the slope-gradient method. Table 1 shows the results obtained using the LiDAR technique to analyze the two periods. After the typhoon event, the flooded land area increased by 63%; the slope was also influenced by the materials transported from the upper stream.

The slope-based roughness index reveals a smoother surface after the disaster; the predisaster period exhibited higher median slope values than did the postdisaster period (Fig. 5).

According to a analysis of the changes in the riverbed area, (Fig. 6) the typhoon delivered a high amount of materials from the upper reach, and the landslide materials comprised the
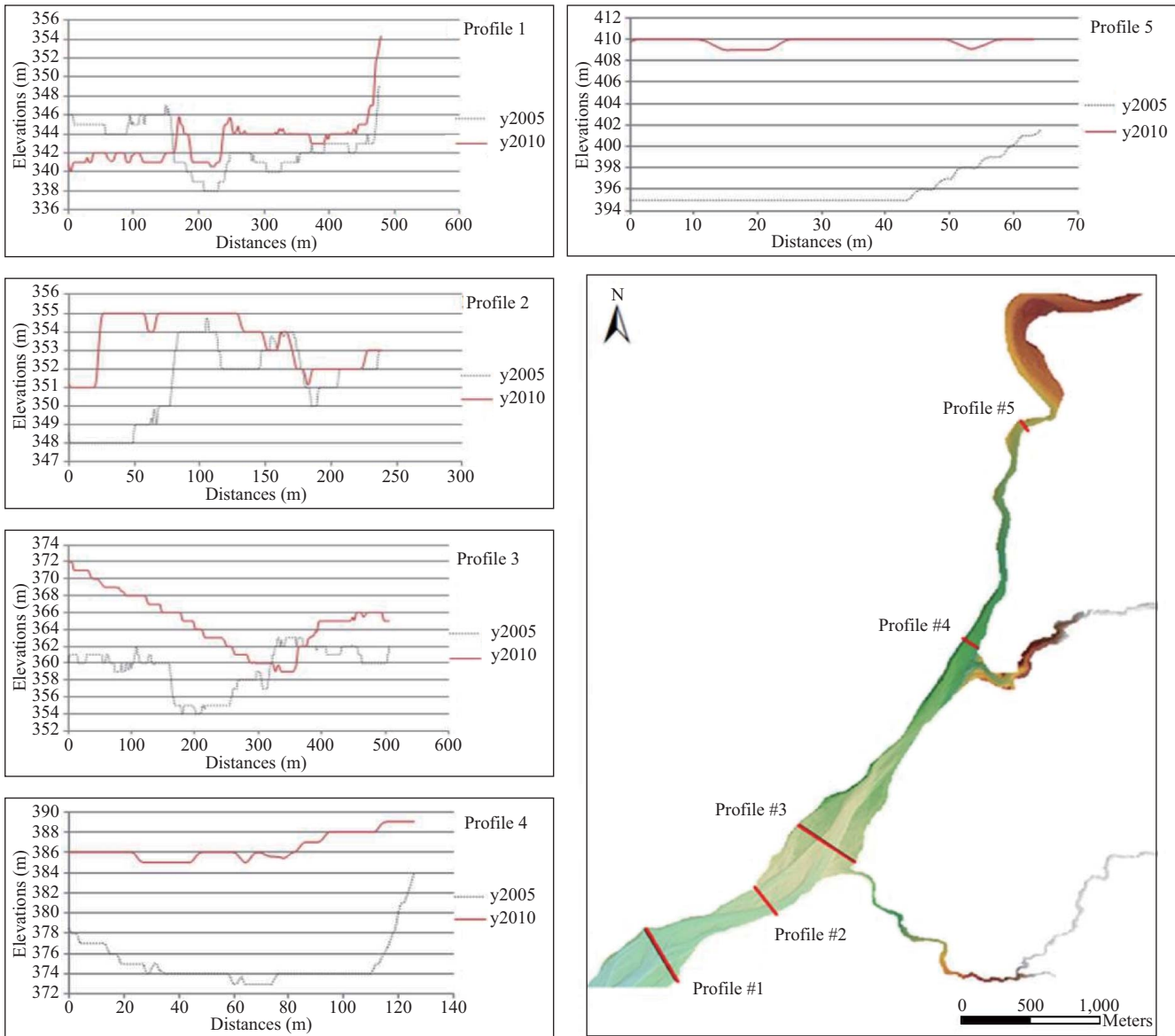
Fig. 7. Comparison the disaster effect exerted by channel morphologies on the riverbed.

most substantial contribution to the riverbed, of which the net gain was greater than the net loss (Table 1).

Fig. 7 shows the cross-sectional profile surveying results. All of the profiles indicate that the postdisaster riverbed elevation increased. The maximal elevation increase exceeded 10 m. In addition, the profiles indicated that the major elevation change occurred in the upper reach. The wide river channel afforded a large sediment deposition space and may have exhibited higher elevation values in the upper reach (Profiles 4 and 5, Fig. 7). In addition, the riverbed morphology was affected by the input of landslide sediments, which deepened the river in the upper reach and broadened the river in the lower reach. The postdisaster river-channel roughness appeared to be smoother than that of the predisaster river-channel roughness. The velocity of the stream flow decreased

when sediment input increased.

V. CONCLUSION

The slope-based roughness index can be used for investigating disasters and river conditions, and river roughness can be treated as a parameter and used in hydrological models. The experimental results indicated that these two methods can reflect the morphologic characteristics of riverbeds. The spectrum pattern revealed the major difference between the slope-based roughness index and the slope-gradient index when describing topographic morphology.

The slope-based roughness appeared smoother than did the slope gradient index, possibly because the slope-based roughness is the standard deviation of residual topography. Thus,

this index can reflect all the features of the entire river, and can show the constant properties of the river channel and the patterns of the riverbed. The postdisaster roughness of the river channel was smoother than the predisaster roughness was; thus, the typhoon deepened the river in the upper reach and broadened the river in the lower reach.

The results indicate that LiDAR data can be considered to be a rapid and useful investigation tools for river condition surveys.

REFERENCES

1. Benda, L. and Dunne, T., "Stochastic forcing of sediment supply to channel networks from landsliding and debris flow," *Water Resources Research*, Vol. 33, No. 12, pp. 2849-2863 (1997).

2. Cavalli, M., Tarolli, P., Marchi, L., and Dalla Fontana, G., "The effectiveness of airborne LiDAR data in the recognition of channel-bed morphology," *Catena*, Vol. 73, No. 3, pp. 249-260 (2008).

3. Chorley, R. J., "The drainage basin as the fundamental geomorphic unit," in: Chorley, R. J. (Ed.), *Water, Earth and Man*, Methuen & Co. Ltd., London, pp. 77-79 (1969).

4. Dhakal, A. S., Amada, T., and Aniya, M., "Landslide hazard mapping and its evaluation using GIS: An investigation of sampling schemes for a grid-cell based quantitative method," *Photogrammetric Engineering and Remote Sensing*, Vol. 66, No. 8, pp. 981-989 (2000).

5. Flores, A. N., Bledsoe, B. P., Cuhaciyan, C. O., and Wohl, E. E., "Channel-reach morphology dependence on energy, scale, and hydroclimatic processes with implications for prediction using geospatial data," *Water Resources Research*, Vol. 42, No. 6, W06412 (2006).

6. Glenn, N. F., Streutker, D. R., Chadwick, D. J., Thackray, G. D., and Dorsch, S. J., "Analysis of LiDAR-derived topographic information for characterizing and differentiating landslide morphology and activity," *Geomorphology*, Vol. 73, Nos. 1-2, pp. 131-148 (2006).

7. Grohmann, C. H., Smith, M. J., and Riccomini, C., "Multiscale analysis of topographic surface roughness in the Midland Valley, Scotland," *IEEE Transactions on Geoscience and Remote Sensing*, Vol. 49, No. 4, pp. 1200-1213 (2011).

8. Horn, B. K. P., "Hill shading and the reflectance map," *Proceedings of the IEEE*, Vol. 69, No. 1, pp. 14-47 (1981).

9. Lenzi, M. A., "Step–pool evolution in the Rio Cordon, northeastern Italy," *Earth Surface Processes and Landforms*, Vol. 26, No. 9, pp. 991-1008 (2001).

10. Li, Y. Y., *Site Geology and its Implication in the Initiation of Hsiaolin Catastrophic Landslide, Kaohsiung City, Taiwan*, Master Thesis, Department of Earth Sciences, National Cheng Kung University, Tainan, Taiwan (2011).

11. Lillesand, T., Kiefer, R. W., and Chipman, J., *Remote Sensing and Image Interpretation*, John Wiley & Sons, University of Wisconsin, Madison (2008).

12. Mark, D. M., "Geomorphometric parameters: a review and evaluation," *Geografiska Annaler Series A, Physical Geography*, Vol. 57, No. 3/4, pp. 165-177 (1975).

13. Mason, D. C., Cobby, D. M., Horritt, M. S., and Bates, P. D., "Floodplain friction parameterization in two-dimensional river flood models using vegetation heights derived from airborne scanning laser altimetry," *Hydrological Processes*, Vol. 17, No. 9, pp. 1711-1732 (2003).

14. McKean, J. and Roering, J., "Objective landslide detection and surface morphology mapping using high-resolution airborne laser altimetry," *Geomorphology*, Vol. 57, Nos. 3-4, pp. 331-351 (2004).

15. Montgomery, D. R. and Buffington, J. M., "Channel-reach morphology in mountain drainage basins," *Geological Society of America Bulletin*, Vol. 109, No. 5, pp. 596-611 (1997).

16. Sharpnack, D. and Akin, G., "An algorithm for computing slope and aspect from elevations," *Photogrammetric Engineering and Remote Sensing*, Vol. 35, No. 3, pp. 247-248 (1969).

17. Zhou, Q. and Liu, X., "Analysis of errors of derived slope and aspect related to DEM data properties," *Computers & Geosciences*, Vol. 30, No. 4, pp. 369-378 (2004).